



**HAL**  
open science

# A HELIUM NanoDroplet Isolation (HENDI) investigation of the weak hydrogen bonding in the propyne dimer (CH<sub>3</sub>CCH)<sub>2</sub>

A. Gutiérrez-Quintanilla, M. Briant, E. Mengesha, M.-A. Gaveau, J.-M. Mestdagh, B. Soep, C. Crépin, L. Poisson

## ► To cite this version:

A. Gutiérrez-Quintanilla, M. Briant, E. Mengesha, M.-A. Gaveau, J.-M. Mestdagh, et al.. A Helium NanoDroplet Isolation (HENDI) investigation of the weak hydrogen bonding in the propyne dimer (CH<sub>3</sub>CCH)<sub>2</sub>. *Physical Chemistry Chemical Physics*, 2018, 20 (45), pp.28658 - 28666. 10.1039/C8CP04738C . cea-01934850

**HAL Id: cea-01934850**

**<https://cea.hal.science/cea-01934850>**

Submitted on 26 Feb 2024

**HAL** is a multi-disciplinary open access archive for the deposit and dissemination of scientific research documents, whether they are published or not. The documents may come from teaching and research institutions in France or abroad, or from public or private research centers.

L'archive ouverte pluridisciplinaire **HAL**, est destinée au dépôt et à la diffusion de documents scientifiques de niveau recherche, publiés ou non, émanant des établissements d'enseignement et de recherche français ou étrangers, des laboratoires publics ou privés.



Cite this: *Phys. Chem. Chem. Phys.*,  
2018, 20, 28658

# A Helium NanoDroplet Isolation (HENDI) investigation of the weak hydrogen bonding in the propyne dimer (CH<sub>3</sub>CCH)<sub>2</sub>

A. Gutiérrez-Quintanilla,<sup>ab</sup> M. Briant,<sup>\*c</sup> E. Mengesha,<sup>c</sup> M.-A. Gaveau,<sup>ib</sup>  
J.-M. Mestdagh,<sup>id</sup> B. Soep,<sup>id</sup> C. Crépin<sup>id</sup><sup>a</sup> and L. Poisson<sup>id</sup><sup>c</sup>

A Helium Nanodroplet Isolation (HENDI) experiment was performed to explore the absorption spectra of the propyne monomer (CH<sub>3</sub>CCH), dimer and (CH<sub>3</sub>CCH)<sub>≥3</sub> multimers in the vicinity of the CH stretch region  $\nu_1$  of the monomer. *Ab initio* calculations were performed at the MP2 level to document the potential energy surface of the dimer. This provided the necessary parameters to simulate the absorption spectrum of the dimer and thus facilitate the interpretation of the experiment. The central result was to observe three isomers of the dimer, hence reflecting the complexity of the weak CH $\cdots\pi$  H-bonding when several H-donors are at play.

Received 25th July 2018,  
Accepted 25th October 2018

DOI: 10.1039/c8cp04738c

rsc.li/pccp

## 1 Introduction

Hydrogen bonding is a well documented attractive interaction between two polar groups. It received an accurate definition from IUPAC: “a form of association between an electronegative atom and a hydrogen atom attached to a second, relatively electronegative atom”.<sup>1</sup> Accordingly, a positively polarized hydrogen atom in one group interacts with an electronegative atom in the other. A text book example is the OH $\cdots$ O interaction between two water molecules. Such “conventional” H-bonds have binding energies ranging between 12 and 30 kJ mol<sup>-1</sup> (1000–2500 cm<sup>-1</sup>). However, the H-bond concept is broader, and weaker H-bonds exist.<sup>2,3</sup> Nishio used the hard/soft acid/base concept to distinguish four classes of H-bonds whether the H-atom donor belongs to a hard (HA) or soft (SA) acid group and the acceptor to a hard (HB) or soft (SB) base.<sup>4</sup> “Conventional” H-bonds belong to the HA/HB class and the weakest H-bonds to SA/SB. The binding energies drop to 6–11 kJ mol<sup>-1</sup> (500–900 cm<sup>-1</sup>) in the latter case.

Weak H-bonds of the SA/SB class exist between a C–H donor and the  $\pi$  electrons of a CC triple bond (the CH $\cdots\pi$  H-bonds). Their weak strength and soft geometry constraint reflect a subtle balance between electrostatic, exchange repulsion, polarization, charge transfer and dispersion. When such a H-bond is sole at play

as in acetylenic dimers (*e.g.* (HCCH)<sub>2</sub> or (CH<sub>3</sub>CCH)<sub>2</sub>), floppy structures and/or several conformers are expected. Documenting such dimers experimentally offers a stringent test for the calculations, which are still a challenge. This was exemplified recently for the very floppy T-shaped acetylene dimer (HCCH)<sub>2</sub>. Leforestier *et al.* calculated the potential energy surface (PES) describing this dimer by combining the symmetry-adapted intermolecular perturbation method with the density functional theory (DFT-SAPT).<sup>5</sup> This served to simulate a microwave absorption spectrum which was compared with experimental data. Ultimately, the PES was refined for an excellent agreement within  $\sim 1$  MHz between the experimental and the simulated spectra. Later, the refined PES served to rationalize an experimental investigation performed in the present laboratory where the large amplitude deformations of (HCCH)<sub>2</sub> within helium droplets were explored.<sup>6</sup>

The situation with (HCCH)<sub>2</sub> was fairly simple, since a single conformer had to be considered.<sup>5,7</sup> A more complex situation is addressed here with the propyne dimer (CH<sub>3</sub>CCH)<sub>2</sub> where several conformers are expected. Two different CH $\cdots\pi$  H-bonds may contribute indeed to the stability of (CH<sub>3</sub>CCH)<sub>2</sub> whether CH or CH<sub>3</sub> acts as the H-donor in the H-bond. Documenting their relative strength for stabilizing isomers is an issue.

The present work investigates the structure of the propyne dimer by performing infrared absorption spectroscopy near the C–H stretch region  $\nu_1$  of the propyne moiety, a A-type transition showing P, Q and R branches. The experiment is conducted using the Helium Nanodroplet Isolation (HENDI) technique in a configuration where the hosted species is deposited in the droplet by a collisional pick-up. The power of associating the HENDI and pick-up techniques is reviewed extensively.<sup>8–12</sup>

<sup>a</sup> Institut des Sciences Moléculaires d'Orsay (ISMO), UMR 8214, CNRS, Univ. Paris-Sud, Université Paris Saclay, F-91405 Orsay, France

<sup>b</sup> Instituto Superior de Tecnologías y Ciencias Aplicadas (InSTEC), Universidad de La Habana. Ave. Salvador Allende No. 1110, Quinta de los Molinos, La Habana 10400, Cuba

<sup>c</sup> LIDYL, CEA, CNRS, Université Paris-Saclay, CEA Saclay, F-91191 Gif-sur-Yvette, France. E-mail: marc.briant@cea.fr

Actually, the association of these two techniques appears as a dedicated tool to investigate the IR spectroscopy of weakly bound complexes: homodimers such as that of acetylene;<sup>6</sup> heterodimers such as glycine/water complexes;<sup>13</sup> complexes involving radical such as allyl or benzyl/water complexes.<sup>14,15</sup> These works follow the pioneering activity of Roger Miller, who first explored the spectroscopy of the weakly H-bonded dimer and trimer of imidazole in helium nanodroplet.<sup>16,17</sup> The same technique served also to document the spectroscopy of the T-shaped benzene dimer where a  $\text{CH}\cdots(\text{aromatic})\pi$  H-bond is at play.<sup>18</sup>

In the present context where propyne dimers are studied, the sequential character of the pick-up is especially well adapted. Two molecules, which are deposited one after the other in the same droplet, are expected to cool down internally at the low droplet temperature (0.38 K) before they associate gently in the first minimum of the PES that is met, even if it is not the most stable one. Statistically, many (if not all) minima of a complex PES will be explored, hence allowing their spectroscopic characterization.

The present work is complemented by *ab initio* calculations to overview the PES, calculate harmonic vibrational frequencies in each PES minimum and guide the interpretation.

## 2 Experimental setup

The experimental setup has been described already.<sup>19</sup> It associates a molecular beam carrying helium droplets (average size of a few thousands atoms), a pickup chamber to deposit the propyne molecules on the droplets and a tunable infrared optical parametric oscillator laser (linewidth 1 MHz). The laser is passing through a multi-pass mirror assembly for exciting the species which are hosted in the helium droplets. The helium droplets are generated by nucleation in a supersonic expansion (5  $\mu\text{m}$  diameter nozzle) with a stagnation pressure and temperature of 14 bar and 10.8 K, respectively.

When several propyne molecules are hosted by the same helium droplet, they are believed to associate together and form molecular assemblies. The calculations performed in the present work (see below) indicate indeed a binding energy of several hundred wavenumbers for the propyne dimer, therefore much larger than the expected propyne-He binding energy, the droplet temperature (0.38 K, *i.e.*  $0.26\text{ cm}^{-1}$ )<sup>20</sup> or the He-He well depth ( $D_e = 7.4\text{ cm}^{-1}$ ).<sup>21</sup>

An experiment consists in monitoring the flux of helium droplet while scanning the laser over the  $3300\text{--}3336.0\text{ cm}^{-1}$  range. When the laser is tuned to a transition of a hosted species (single molecule or molecular assembly), the latter is excited and the resulting vibrational energy relaxes to the droplet, which evaporates. The corresponding decay of the droplet flux reflects the absorption spectrum of the hosted species. Here, the droplet flux is monitored by recording the  $\text{He}_2^+$  signal in a quadrupole mass spectrometer coupled with a lock-in amplifier.

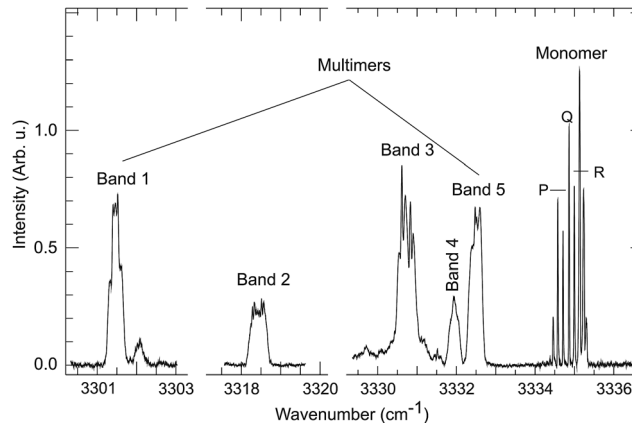


Fig. 1 Absorption spectrum of propyne in helium nanodroplets. Only the three regions where the propyne monomer or multimers absorb are shown in the figure. The assignments which label the spectral bands are justified in the text.

## 3 Experimental results

Fig. 1 reports the absorption spectrum measured experimentally. The horizontal scale of the figure is limited to the three regions where a significant absorption signal is observed. The red side of the spectrum, below  $3333.5\text{ cm}^{-1}$ , looks very different from the blue side where a series of narrow lines is observed.

### 3.1 The narrow band series: absorption by a propyne monomer

The series of narrow bands observed in the upper energy region of Fig. 1 ( $3334.4\text{--}3335.5\text{ cm}^{-1}$ ) reproduces the lines observed by Nauta and Miller who run the first HENDI experiment on the propyne molecule.<sup>22</sup> These lines were assigned to the P, Q and R transitions of the propyne monomer as labeled in Fig. 1.

We followed this assignment and simulated the absorption spectrum in the  $3334.3\text{--}3335.5\text{ cm}^{-1}$  energy region, using PGOPHER, a general program suite for simulating rotational, vibrational and electronic spectra.<sup>25</sup> Appropriate inputs into PGOPHER allowed us dealing with the present  $\text{C}_{3v}$  symmetric top molecule. The comparison between the experimental spectrum (taken from Fig. 1) and the simulated one is shown in Fig. 2. The simulation includes a  $0.01\text{ cm}^{-1}$  Lorentzian linewidth to account phenomenologically for the broadening due to the interaction between propyne and helium environment. Note that the laser width (1 MHz) is negligible at this scale.

As always with HENDI spectroscopy, the spectroscopic constants of the isolated molecule need to be replaced by effective constants to account phenomenologically for the coupling between the ro-vibrational levels of the hosted molecule, the non-superfluid component of the droplet and collective excitations in the remaining part of the droplet.<sup>9,12</sup> The constants which served to best fit the spectral lines observed in Fig. 2 are shown in the last column of Table 1 where they are compared to those found by Nauta and Miller in their HENDI experiment (third column) and to those of the isolated propyne molecule (second column). The dash in the third column of the table indicates the constants which were not

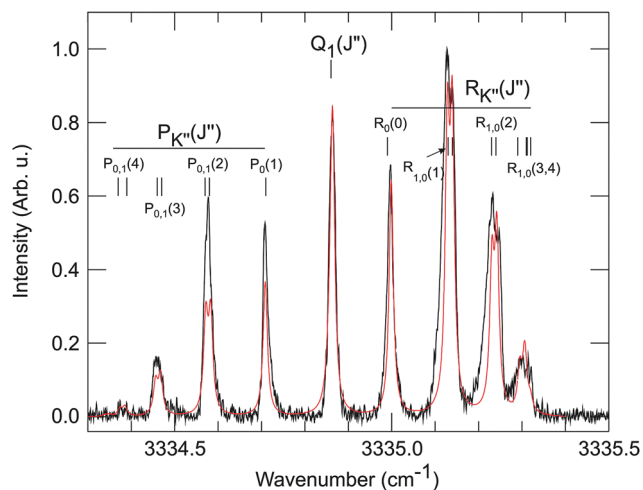


Fig. 2 Absorption spectrum assigned to the propyne monomer (black curve, taken from Fig. 1) compared with the simulation performed with the constants listed in Table 1 (red curve).

**Table 1** Spectroscopic constants ( $\text{cm}^{-1}$ ) of the propyne monomer, either isolated (column 2) or embedded in helium droplets (columns 3 and 4). The column 4 values were adjusted to best fit the lines assigned to the monomer in Fig. 1. The uncertainty on the last digit is given between parentheses. Note that the fit is only sensitive to the difference  $A'' - A'$ . The  $A''$  value in column 4 is taken arbitrarily to be that of isolated propyne (column 2)

	Isolated	He-droplet	
		<sup>c</sup>	(Present work)
$A''$	5.308410 <sup>a</sup>	—	5.308410(0)
$B''$	0.285059 <sup>a</sup>	0.0741	0.0742(5)
$\Delta_J''$	$9.80462 \times 10^{-8}$ <sup>a</sup>	0.0005	0.00050(3)
$\Delta_{JK}''$	$5.45117 \times 10^{-6}$ <sup>a</sup>	—	0
$\Delta_K''$	$9.83 \times 10^{-5}$ <sup>a</sup>	—	0
$\nu_1$	3335.0594 <sup>b</sup>	3334.90	3334.855(3)
$A'$	5.31714 <sup>b</sup>	—	5.3185(10)
$B'$	0.2843846 <sup>b</sup>	0.0731	0.0729(3)
$\Delta_J'$	—	0.0005	0.00050(3)
$\Delta_{JK}'$	—	—	0
$\Delta_K'$	—	—	0

<sup>a</sup> Horneman *et al.*<sup>23</sup> <sup>b</sup> McIlroy and Nesbitt.<sup>24</sup> <sup>c</sup> Nauta and Miller.<sup>22</sup>

documented by Nauta and Miller.<sup>22</sup> Note that the information on the  $A''$  and  $A'$  spectroscopic constants is not very accurate since their adjustment acts on the small, almost unresolved, K-splitting of the P and R spectral lines.

### 3.2 Scaling the average number $\langle n_{\text{Propyne}} \rangle$ of propyne molecules per droplet with the pickup pressure $P_{\text{Propyne}}$

The lines that have just been discussed are due to the absorption of the propyne monomer hosted in the droplets. As a first approximation, the Poisson statistics applies for the pick-up process.<sup>26</sup> Hence, the intensity of these lines must behave as the first order Poisson distribution ( $P_1(\langle n_{\text{Propyne}} \rangle) = \langle n_{\text{Propyne}} \rangle \times \exp(-\langle n_{\text{Propyne}} \rangle)$ ) when the average number  $\langle n_{\text{Propyne}} \rangle$  of propyne molecules per droplet is varied. A simple proportionality

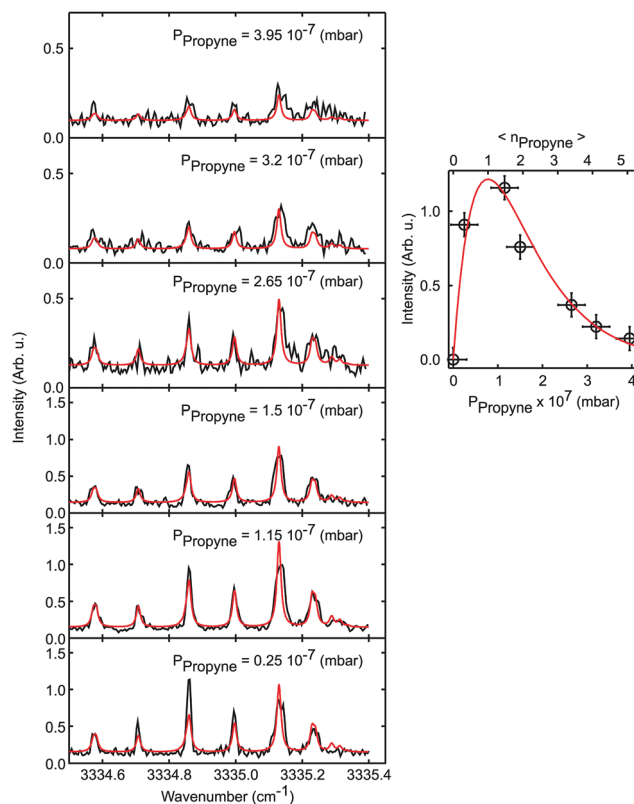


Fig. 3 The left column shows the fit (in red) of the absorption spectra (in black) taken at various propyne pick-up pressures in the monomer region of the spectrum. The vertical scale is not the same in the upper three panel of this column. The right column is a Poisson plot showing that the intensity of the simulated spectra (open circles) varies as the first order Poisson distribution (red curve) when  $P_{\text{Propyne}}$ , the pick-up pressure, is varied. The upper scale of the figure shows the correspondence between  $P_{\text{Propyne}}$  and  $\langle n_{\text{Propyne}} \rangle$ , the average number of propyne molecules deposited per droplet.

factor scales  $\langle n_{\text{Propyne}} \rangle$  with the propyne pickup pressure  $P_{\text{Propyne}}$ . This is achieved in Fig. 3, which is described now.

The six panels in the left column of Fig. 3 show the monomer region of the absorption spectra for different pickup pressures  $P_{\text{Propyne}}$  (black curves). As a compromise between signal/noise ratio and acquisition time, these spectra were recorded with a lower sampling resolution than the spectrum shown in Fig. 2. Hence, the K-splitting of the P and R spectral lines is no longer visible. The red curve in each panel of Fig. 3 shows the simulated spectrum that was discussed in the previous section after its intensity was adjusted to best fit the experimental curve. These adjusted intensities are plotted as a function of  $P_{\text{Propyne}}$  in the right column of Fig. 3. The red curve passing through the experimental point is a fit by a first order Poisson distribution. It allowed us scaling  $\langle n_{\text{Propyne}} \rangle$  (top scale) with  $P_{\text{Propyne}}$  (bottom scale).

### 3.3 The broad band series: absorption by propyne multimers

The bands which appear on the red side of the monomer lines in Fig. 1 are tentatively assigned to absorption by the propyne dimer. To check this assumption, the absorption region of

“Bands” 3, 4 and 5 was studied as a function of the pick-up pressure. The corresponding spectra are shown in the first column of Fig. 4 for six pick-up pressures. Apparently, the sub-band structure of “Band” 3 (and “Bands” 4 and 5 in a lesser extent) is more pronounced at low pickup pressure. This suggests that the structured “Bands” 3, 4 and 5, which are dominant when  $P_{\text{Propyne}} \approx 1.15 \times 10^{-7}$  mbar, are superimposed on an “unstructured” component, which grows at their expense when  $P_{\text{Propyne}}$  increases.

The very structured “Band 3” appears as a series of 6 Gaussian sub-bands, “Band 4” as a single peak and “Band 5” as a triplet. These features are adequately fitted using the Gaussian functions listed in Table 2. Finally, the “Unstructured component” was modeled as three broad features approximately underneath each structured band. They are centred at  $3330.4 \text{ cm}^{-1}$  (width  $1.9 \text{ cm}^{-1}$ ),  $3330.8 \text{ cm}^{-1}$  (width  $0.4 \text{ cm}^{-1}$ ) and  $3332.3 \text{ cm}^{-1}$  (width  $0.6 \text{ cm}^{-1}$ ) in the ratio 1:0.4:0.04.

The dark blue curve in the left panels of Fig. 4 shows the contribution of the “Unstructured component”. The green curve shows that of the three structured components (“Bands” 3, 4 and 5). The relative intensity of the four components, “Bands” 3, 4, 5 and “Unstructured component” were used as independent parameters for their sum (shown as the red curve in the figure) best fits the experimental spectra. The right panels of Fig. 4 show Poisson plots where these intensities

Table 2 Gaussian sub-bands which describe “Band 3, 4” and “5”

Band 3		Band 4		Band 5	
Centre ( $\text{cm}^{-1}$ )	Width ( $\text{cm}^{-1}$ )	Centre ( $\text{cm}^{-1}$ )	Width ( $\text{cm}^{-1}$ )	Centre ( $\text{cm}^{-1}$ )	Width ( $\text{cm}^{-1}$ )
3330.56	0.075	3331.99	0.22	3332.40	0.12
3330.64	0.045			3332.51	0.09
3330.74	0.10			3332.63	0.13
3330.85	0.045				
3330.93	0.055				
3331.0	0.055				

are plotted as a function of  $\langle n_{\text{Propyne}} \rangle$ . Of course,  $\langle n_{\text{Propyne}} \rangle$  was deduced from  $P_{\text{Propyne}}$  using the scaling law derived in Section 3.2.

The red, green and blue solid curves which appear in the Poisson plots (right panels of Fig. 4) show the Poisson distributions  $P_i(\langle n_{\text{Propyne}} \rangle) = \frac{1}{i!} \langle n_{\text{Propyne}} \rangle^i \exp(-\langle n_{\text{Propyne}} \rangle)$  of first, second and third order ( $i = 1, 2, 3$ , respectively). They describe the variation of a signal due to droplets carrying a monomer, a dimer or a trimer, respectively. The pink curve shows the quantity  $1 - P_0(\langle n_{\text{Propyne}} \rangle) - P_1(\langle n_{\text{Propyne}} \rangle) - P_2(\langle n_{\text{Propyne}} \rangle)$ . It mimics a signal due to droplets carrying a trimer and larger multimers. The maximum intensity of these curves is set to one for an easier comparison with the experimental data.

The experimental points describing the “Unstructured component” (bottom panel) follow the blue curve or, within experimental uncertainties, the pink curve. This component is therefore associated with absorption by propyne trimers and possibly by larger multimers. Although the dispersion of the experimental points is quite large, the other panels suggest that the “Band” 3, 4 and 5 intensities follow the green curve, hence confirming their assignment to the absorption by propyne dimers.

The dispersion of the experimental points about the Poisson curve in the right column of Fig. 4 illustrates that these experiments are difficult because of various unstabilities in our setup. The data acquisition for Poisson plots lasts indeed several hours. No Poisson plot was attempted for the absorption “bands” 1 and 2. They are far from the monomer lines (which are necessary to scale the pick-up pressure) and cannot be recorded with them easily.

## 4 Calculations

The experimental results were complemented by *ab initio* calculations to follow the potential energy of the propyne dimer when varying the angle between the symmetry axes of the propyne moieties. The calculation were performed using the MOLPRO 2010.1 suite of quantum chemistry packages.<sup>27</sup>

### 4.1 Description of the propyne monomer

The first step of the calculations was to describe the  $\text{CH}_3\text{CCH}$  monomer. Its geometry is believed to reflect that of the  $\text{CH}_3\text{CCH}$  moieties in the dimer since the H-bond is weak and

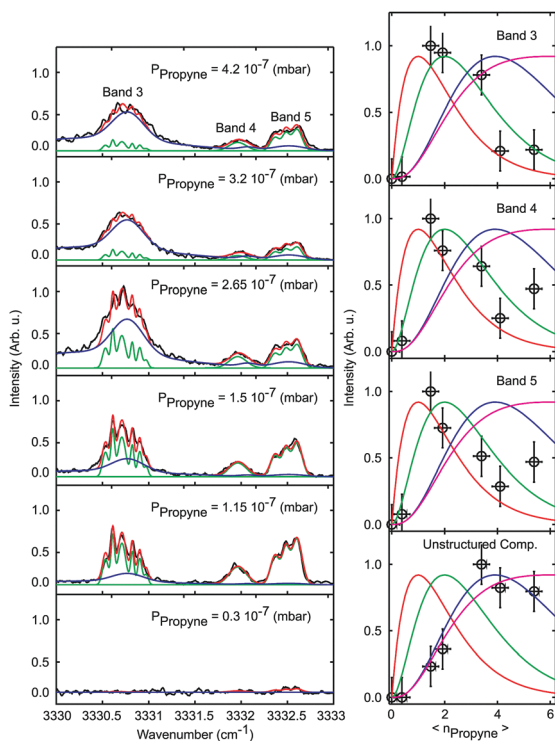


Fig. 4 Same caption as Fig. 3 for the multimer region of the spectrum. The red, green and blue solid curves in the second column show the Poisson distributions  $P_i(\langle n_{\text{Propyne}} \rangle)$  of first, second and third order ( $i = 1, 2, 3$ , respectively). The pink curve shows the quantity  $1 - P_0(\langle n_{\text{Propyne}} \rangle) - P_1(\langle n_{\text{Propyne}} \rangle) - P_2(\langle n_{\text{Propyne}} \rangle)$ . The maximum intensity of these curves is set to one for an easier comparison with the experimental data.

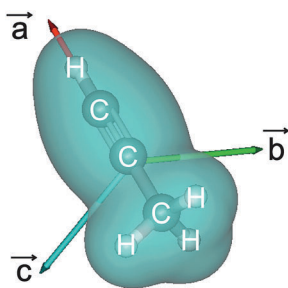


Fig. 5 Propyne molecule, principal molecular axes ( $\vec{a}$ ,  $\vec{b}$  and  $\vec{c}$ ) and electronic density. The later is provided by the RHF orbitals of the MP2/aug-cc-pVTZ calculation and represents 99% of the full electron population.

is not likely to affect dramatically the shape of the  $\text{CH}_3\text{CCH}$  moieties.

The present description of the  $\text{CH}_3\text{CCH}$  monomer follows the high level one of El Idrissi *et al.*<sup>28</sup> Accordingly, the geometry of  $\text{CH}_3\text{CCH}$  was optimized at the second order Møller–Plesset (MP2) level of theory,<sup>29</sup> using the aug-cc-pVTZ correlation consistent polarized basis set of Kendall *et al.*<sup>30,31</sup> The electronic density about the  $\text{CH}_3\text{CCH}$  skeleton is shown in Fig. 5.

#### 4.2 Coordinate system of the propyne dimer

When calculating the PES of the acetylene dimer Leforestier *et al.* showed that its equilibrium structure is planar.<sup>5</sup> Out-of-plane deformations break indeed the H-bond which stabilizes the dimer. As a reminiscence of this effect, the skeleton formed by the two  $\text{C}\equiv\text{CH}$  groups in the  $(\text{CH}_3\text{C}\equiv\text{CH})_2$  dimer is believed to be planar. This defines a skeleton plane of  $x$ ,  $y$  coordinate. A  $\text{CH}_3\text{CCH}$  molecule is placed at the origin of the coordinate with one of the H-atoms of the methyl group in the skeleton plane (see Fig. 6). Four coordinates remain for describing the dimer:  $x_M$  and  $y_M$  locate the centre M of the other  $\text{C}\equiv\text{C}$  group;  $\alpha$  is the angle between the symmetry axes of the two  $\text{CH}_3\text{CCH}$  molecules;  $\phi$  is the azimuthal angle of the  $\text{CH}_3$  group which is still free to rotate.

#### 4.3 Stationary points in the propyne dimer surface

The PES of the propyne dimer was explored along the  $\alpha$  coordinate while optimizing the 3 other coordinates. The following strategy was chosen as a compromise between accuracy and computational effort. First, a quick look was given to the PES

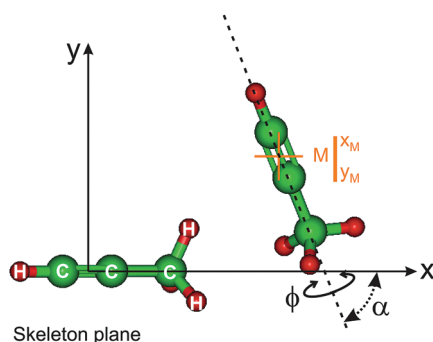


Fig. 6 Coordinate system used to describe the  $(\text{CH}_3\text{CCH})_2$  dimer.

Table 3 Angle  $\alpha$  between the symmetry axes of the  $\text{CH}_3\text{CCH}$  molecules in the propyne dimer and corresponding binding energy for various calculation levels. The energies are referred to the dissociation when the two propyne moieties are at infinite separation

Stationary point	$\alpha$ (degrees)	Type of calculation		
		avdz <sup>a</sup> (cm <sup>-1</sup> )	avdz+bsse <sup>b</sup> (cm <sup>-1</sup> )	avtz+bsse <sup>c</sup> (cm <sup>-1</sup> )
$m_1$	-185.3	-1242	-682	-832
$ts_1$	-127.8	-766	-328	-414
$m_2$	-98.1		-358	-448
	-62.5	-857	-355	-453
$ts_2$	-3.8	-375		
	-8.8		-44	-97
$m_3$	48.6	-1165	-667	-808
$ts_3$	136.7	-354	-43	-99

<sup>a</sup> aug-cc-pVDZ basis set and no BSSE correction. <sup>b</sup> aug-cc-pVDZ basis set including the BSSE correction. <sup>c</sup> aug-cc-pVTZ basis set including the BSSE correction.

using the aug-cc-pVDZ double zeta basis set and sampling angle  $\alpha$  between  $-180$  and  $+180$ . Three minima separated by three transition states were found. Quantitative information on these stationary points are reported in Table 3. No correction was performed at this step for the basis set superposition error (BSSE). The next step is a full optimization of the four coordinates in the region of these stationary points in a calculation which includes the Boys and Bernardi counterpoise correction of the BSSE.<sup>32</sup> The corresponding results are reported in Table 3 also. Finally, a refine calculation is performed at each stationary point, using the aug-cc-pVTZ triple zeta basis set and the density fitting option provided by the MOLPRO package. Accordingly, an appropriate combination of cc-pVQZ JK and aug-cc-pVTZ MP2-fitting basis sets were used. The corresponding results are shown in Table 3 and Fig. 7.

Table 3 makes clear that the effect of the BSSE correction is quantitatively significant although the BSSE-uncorrected results follow qualitatively the corrected ones. This indicates that the potential landscape with 3 minima and transition states is fairly stable whatever the level of theory and can be considered as reliable for discussing the experimental results.

The shape of the dimer at the six stationary points is shown in Fig. 7. The most stable isomers  $m_1$  and  $m_3$  are stabilized by two  $\text{CH}\cdots\pi$  bond whereas a single  $\text{CH}\cdots\pi$  bond appears in the less stable isomer  $m_2$ . The distance between the two propyne molecules does not change dramatically from one isomer to the other. Quantitative information on the stationary points are reported in Table 3 (relative energies at various calculation levels) and 4 (geometric parameters, rotational constants and C–H stretch vibrational constants).

Within  $\approx 5^\circ$ , the two  $\text{CH}_3\text{CCH}$  molecules are approximately antiparallel in isomer  $m_1$ . With this geometry, both  $\text{CH}_3$  groups can interact with the electron cloud of a  $\text{C}\equiv\text{C}$  groups. Two  $\text{CH}\cdots\pi$  bonds are formed. The similar role played by the  $\text{CH}_3\text{CCH}$  molecules in this isomer is also revealed by the columns labeled “Frequency” and “Intensity” in Table 4. Two C–H transitions appear with almost equal frequencies but very different

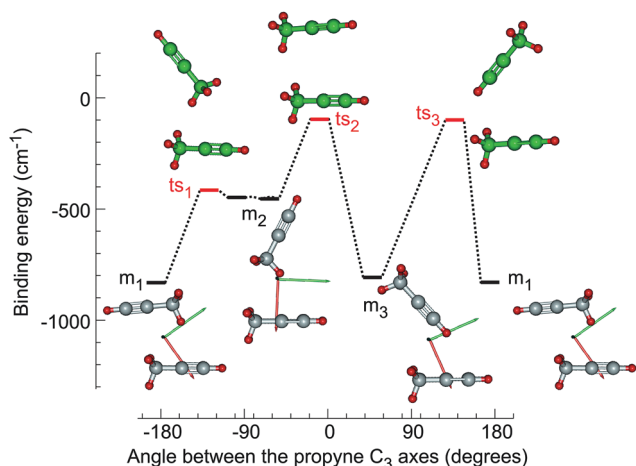


Fig. 7 Potential energy of the propyne dimer along the  $\alpha$  coordinate. The results of the calculations, performed at the MP2/aug-cc-pVTZ level theory including the BSSE correction, are reported in black full line (see text for details). The shape of the dimer is shown above the corresponding minima  $m_1$ ,  $m_2$  and  $m_3$  (the in-plane principal inertia axes are indicated as red and green arrows) and transition states  $ts_1$ ,  $ts_2$  and  $ts_3$ .

intensities. They correspond to the symmetric and antisymmetric stretch of the two C–H bonds.

The situation is different with isomer  $m_3$  since the H-atom donors which form the two  $\text{CH}\cdots\pi$  bonds are of different nature. One is the CH acetylenic group and the other the  $\text{CH}_3$  group. Not surprisingly, the two C–H stretch frequencies are very different in Table 4. That of lower frequency is associated with the CH group which is involved in a H-bond. Apparently, this isomer is slightly less stable than  $m_1$  whatever the level of theory.

The transition states  $ts_2$  and  $ts_3$  have energies slightly below the dissociation of the dimer. The double  $\text{CH}\cdots\pi$  bond is essentially broken in these stationary points and the remaining binding energy is probably of almost pure van der Waals origin. Note that the location of the  $ts_2$  is changed slightly between  $\alpha = -3.8$  and  $\alpha = -8.8$  when the BSSE correction is included.

We turn now to the isomer  $m_2$ . Its binding energy is about half that of isomers  $m_1$  and  $m_3$ . This reflects what is apparent on its structure: a single  $\text{CH}\cdots\pi$  bond is present. The latter is formed with a  $\text{CH}_3$  group as the H-atom donor. It is separated from isomer  $m_1$  by a very small barrier. Importantly, the geometry optimization was difficult to converge for this isomer, presumably because the potential energy surface is fairly flat in this geometrical region. Although the two  $\text{CH}_3\text{CCH}$  molecules do not play the same role in this isomer, Table 4 shows fairly close frequencies with similar intensities for their CH stretch excitation. This simply reflects that the CH groups do not participate to the H-bond and thus have an equivalent position regarding the stretch.

Finally, a possible fourth minimum where the CH acetylenic group acts as the H-atom donor (an approximately T-shaped  $\text{CH}_3^-\cdots\text{CCH}\cdots$  isomer) has been searched carefully. Unavoidably, the optimization has converged to the  $m_3$  minimum indicating that no barrier exist along the  $\alpha$  coordinate to allow stabilizing such an isomer in a suspended well. This is in marked contrast with what has just been discussed for isomer  $m_2$ . Presumably, the very small barrier which separates isomer  $m_2$  from  $m_1$  is due to a steric effects that can be understood when observing the electronic density of  $\text{CH}_3\text{CCH}$  in Fig. 5. It is broader at the  $\text{CH}_3$  end of  $\text{CH}_3\text{CCH}$  than at the H end. Apparently, this offers a stable equilibrium position when the  $\text{CH}_3$  end of one propyne molecule makes a bidentate H-bond with the  $\text{C}\equiv\text{C}$  bond of the other molecule. Each acetylenic CH of one propyne molecule does a H-bond with the  $\text{C}\equiv\text{C}$  bond of the other.

## 5 Discussion

From Section 3.3 we know that several components must be distinguished in the left part of the Fig. 1 spectrum, that due to the absorption by droplets carrying propyne multimers. Each component is discussed now.

According to the Poisson analysis, besides the “unstructured component” which is assigned to the absorption by multimers larger than the dimer, five bands (noted band 1–5) originate

Table 4 Calculated spectroscopic constants and structural parameters of the  $(\text{CH}_3\text{CCH})_2$  isomers  $m_1$ ,  $m_2$  and  $m_3$ . The rotational constants correspond to the geometry optimization performed at the MP2/aug-cc-pVDZ level, including the BSSE correction. The C–H stretch frequencies were obtained after a full geometry optimization at the MP2/aug-cc-pVDZ level without BSSE correction. The level of these calculations is a compromise between accuracy and feasibility of the necessary full optimizations in a reasonable time (typically one day for each isomer). The angles  $\alpha$  and  $\phi$  are defined in Fig. 6;  $R$  is the distance between the centre of the  $\text{C}\equiv\text{C}$  bond of one propyne molecule and that of the other; % $a$ :% $b$  indicates how the vibrational transition is shared along the principal axes  $a$  and  $b$  (given in percentages)

Isomer	$\alpha$ (degrees)	$\phi$ (degrees)	$R$ (nm)	Rotational constants			Frequency ( $\text{cm}^{-1}$ )	C–H stretch		
				$A$ ( $\text{cm}^{-1}$ )	$B$ ( $\text{cm}^{-1}$ )	$C$ ( $\text{cm}^{-1}$ )		Intensity		% $a$ :% $b$
$m_1$	−185.3	0.0	0.47	0.18	0.050	0.040	3485.12	103.24	100.0	
							3485.32	6.71	6.5	19:81
$m_2$	−62.0	0.0	0.53	0.23	0.035	0.031	3485.49	52.17	65.3	89:11
							3486.61	58.87	73.7	1:99
$m_3$	48.6	0.0	0.41	0.27	0.035	0.031	3460.41	149.05	100.0	99:1
							3472.67	56.12	37.7	17:83

from droplets carrying a propyne dimer. These bands reflect the absorption by the various isomers of the propyne dimer that can be formed in the droplet environment. Their number, five, is consistent with the calculation results reported in Fig. 7 and Table 4. Among the three isomers that are predicted, two of them,  $m_2$  and  $m_3$ , are associated with two C–H stretch frequencies of comparable intensity (see last column of Table 4). In contrast, isomer  $m_1$ , which has the two  $\equiv\text{C-H}$  groups in almost equivalent positions (see Fig. 7), is associated with two almost equal C–H stretch frequencies, one of which only carries a significant oscillator strength. Hence, five absorption lines are predicted for the dimer isomers, in agreement with the observation in Fig. 1.

“Band” 4 is fairly unstructured. It is centred at  $3331.93\text{ cm}^{-1}$  (see Fig. 1). We do the assumption, which will be checked later, that “band” 4 reflects the red transition of isomer  $m_2$ . The latter is predicted at  $3485.49\text{ cm}^{-1}$  (see Table 4). Since vibrational frequencies are almost unchanged in HENDI experiments, this suggests a scaling factor of 0.95594 to match the predicted value with experiment.<sup>†</sup> Using this factor, the predicted stretch frequencies of the other transitions becomes:  $3331.58\text{ cm}^{-1}$  for isomer  $m_1$ ;  $3331.93$  and  $3332.99\text{ cm}^{-1}$  for  $m_2$ ;  $3307.93$  and  $3319.67\text{ cm}^{-1}$  for  $m_3$ . These frequencies match quite nicely with centre of the dimer bands that can be estimated in Fig. 1:  $\approx 3330.7\text{ cm}^{-1}$  for band 3;  $\approx 3331.9$  and  $3332.5\text{ cm}^{-1}$  for bands 4 and 5, respectively;  $3301.5$  and  $3318.4\text{ cm}^{-1}$  for bands 1 and 2, respectively. The agreement between the scaled predictions and these observations ranges between 0 and  $1.25\text{ cm}^{-1}$ , except for the reddest band near  $3301.5\text{ cm}^{-1}$  (band 1) where the prediction is  $6.5\text{ cm}^{-1}$  off the observation. The latter band deserve a specific discussion. In agreement with the experimental observation, the predicted value of  $3307.93\text{ cm}^{-1}$  is much redder than the other absorption band of isomer  $m_3$ . The corresponding CH stretch involves the H-atom which is directly involved in the H-bond. Two explanations may be invoked to account for the discrepancy between the experimental value in the helium environment and the calculation performed on the free dimer. The first one is purely technical. This particular stretch mode is likely anharmonic and therefore badly described in a harmonic description of the vibrational modes. The second explanation refers to the red shifts that were reported by Choi *et al.* when hydrogen bonded complexes are embedded in a helium droplet.<sup>11</sup> Whereas “free” stretches are essentially unaffected by the helium environment, a red shift ranging between  $1.5$  and  $12\text{ cm}^{-1}$  is observed on vibrational modes which carries the hydrogen bond. From this work, a red shift of  $1\text{--}2\text{ cm}^{-1}$  is expected for the mode of isomer  $m_3$  which is predicted at  $3307.93\text{ cm}^{-1}$ . This is less than half the discrepancy with the experiment, which therefore should be considered as partly due to the oversimplified harmonic description of this mode.

We consider that the above agreement justifies the assignment of “band” 4 to the red transition of isomer  $m_2$  and allows

<sup>†</sup> For comparison, the predicted frequency of the propyne monomer at the same level of theory is  $3487.97\text{ cm}^{-1}$ ; the scaling factor would be 0.95616 to match this value with the experiment.

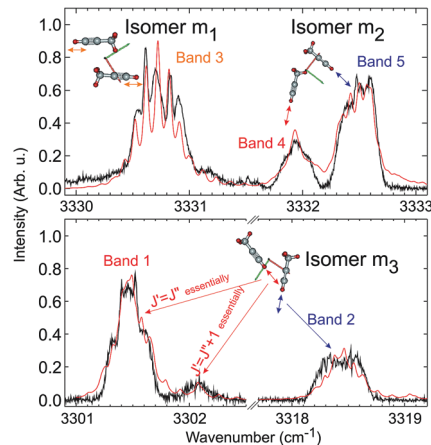


Fig. 8 Fit to the absorption spectrum of propyne in helium nanodroplets. The experimental spectrum (in black) is taken from Fig. 1. The red curve is a simulation as explained in Section 5. The inserts reproduce the geometry of the 3 isomers and assign each observed band to a specific CH stretch.

the full assignment shown in Fig. 8 where “bands” 1 (and its low intensity sub-band) and 2 are assigned to the red and blue transitions of isomer  $m_3$ , “band” 3 to the single transition of  $m_1$  and “bands” 4 and 5 to the two transitions of  $m_2$ .

With the above assignment and the assumption that each isomer behaves as an asymmetric top molecule, we are prepared to simulate the absorption spectrum due to droplets carrying a propyne dimer. As before for the propyne monomer, the spectrum of the propyne dimer was simulated using the PGOPHER program suite.<sup>25</sup> The purpose is to best fit the experimental spectrum by adjusting effective spectroscopic constants to each isomer. To limit the number of parameters to adjust for each isomer, both the ground and excited vibrational states were described by the same set of rotational and distortion constants. The best fit is shown as the red curve in Fig. 8 and compared to the experimental spectrum in black. The effective spectroscopic constants are listed in Table 5.

When comparing Tables 4 and 5, it appears that the effective rotational A constant is a factor 3 to 5 smaller than the prediction for the free dimer. This is in line with what is observed in Table 1 for the rotational constant  $B''$  (or  $B'$ ) of the propyne monomer whether it is free or embedded into the helium droplet (a factor 3.9 smaller). Similarly the effective rotational constants  $B$  and  $C$  are a factor 5 to 20 smaller than the corresponding values for the free dimer. Such very small values of the effective constants for slow rotations reflect the dynamical effect of the non-superfluid component of the droplet. This effect, which is observed in the present work for the propyne monomer and for the 3 isomers of the propyne dimer, has been observed and discussed many times for other molecular species.<sup>9,10,12</sup> It is due to the increase of the molecular moment of inertia when the molecular rotation drives the non-superfluid component of the droplet into movement. Quantitatively, the reduction factors mentioned above are consistent with those observed for slow rotations (rotational constant smaller than  $1\text{ cm}^{-1}$ ) by Callegari *et al.*, when the hosted

**Table 5** Effective spectroscopic constants (in  $\text{cm}^{-1}$  except %a:%b, which is dimensionless) used for the simulation shown as red curve in Fig. 8. The parentheses show the uncertainty on the last digit

	$m_1$	$m_2$		$m_3$	
$\nu = 1$ origin	3330.67	3331.93	3332.47	3301.45	3318.42
%a:%b	0:100 to 20:80	40:60 to 60:40	0:100 to 5:95	40:60 to 50:50	20:80 to 40:60
Width	0.06(1)	0.06(1)		0.06(1)	
$A$	0.055(5)	0.050(5)		0.050(5)	
$B$	0.0025(5)	0.0070(5)		0.0035(5)	
$C$	0.0025(5)	0.0070(5)		0.0035(5)	
$\Delta_K$	0.0004(2)	0.0008(3)		0.0003(2)	
$\Delta_{JK}$	0.0002(1)	0.0004(2)		0.0003(2)	
$\Delta_J$	0.0004(2)	0.0003(2)		0.0004(2)	
$\Phi_K, \Phi_{KJ}, \Phi_{JK}, \Phi_J$	$5 \times 10^{-6}$	$5 \times 10^{-6}$		$5 \times 10^{-6}$	

molecule is bound to the non-superfluid component of the droplet.<sup>9</sup>

It is interesting to compare the effective value of the ratio %a:%b given in Table 5 to the values calculated for the free complex (Table 4). This ratio indicates how the vibrational transition is shared between the principal axes  $a$  and  $b$ . The effective values often deviate substantially from the free complex values. A striking example is met with isomer  $m_1$ . The well resolved structure of the absorption spectrum observed experimentally is typical of a dominant “ $b$ ” transition. The effective ratio %a:%b, which ranges between 0:100 and 20:80, reflects this behaviour. In contrast, the calculation of the free  $m_1$  isomer predicts a significant weight for the  $a$  transition. This may appear as another evidence that the propyne dimer is bound to the non-superfluid component of the droplet. Accordingly, the  $\{a, b, c\}$  nature of the rovibrational transitions is defined by reference to the inertia principal axes of the composite system: hosted dimer + non-superfluid component of the droplet. The latter axes would coincide with those of the free isomer either if the non-superfluid component of the droplet were distributed isotropically about the isomer or if it were matching the geometry of the isomer. The present observations suggests that these conditions do not apply to the  $m_1$  isomer. A rotation of the effective principal axes by ca.  $+15^\circ$  about the  $c$  axis would account for the observation. Similarly a rotation by ca.  $-20^\circ$  and  $+45^\circ$  about the same axis is consistent with the observation of both C–H transitions in isomers  $m_2$  and  $m_3$ , respectively. All together, this suggests a significantly anisotropic distribution of the helium non-superfluid component which does not match with the principal axes of the embedded propyne dimer.

The effective distortion constants  $\Delta_K$ ,  $\Delta_{JK}$  and  $\Delta_J$  found for the three isomers of the propyne dimer in helium droplets have the same order of magnitude as the  $\Delta_K''$  and  $\Delta_K'$  constants of the propyne monomer in the same environment (see Table 1).<sup>‡</sup> The later values are several orders of magnitude larger than those of the corresponding quantities when the propyne molecule is isolated in the gas phase. This has been observed already by Nauta and Miller.<sup>22</sup> Such a behaviour is widespread in HENDI experiments.

<sup>‡</sup> Note that to prevent troubles in the PGOPHER calculation with such large values of  $\Delta_K$ ,  $\Delta_{JK}$  and  $\Delta_J$ , sextic centrifugal distortion constants  $\Phi_K$ ,  $\Phi_{KJ}$ ,  $\Phi_{JK}$  and  $\Phi_J$  were included with a value of  $5 \times 10^{-6} \text{ cm}^{-1}$ . This prevents the energy of the rotational levels to decrease unrealistically at large values of  $J$  and  $K$ .

It received a full theoretical interpretation when the  $\text{C}_2\text{H}_2$  molecule is hosted in helium droplets.<sup>33</sup> Zillich *et al.* used a path-integral correlation function approach and found a quantitative agreement with experiment for the anomalously large effective distortion constant of this molecule in helium droplets. A semi-analytic treatment of the dynamics then reveals that this phenomenon is due to a strong coupling between the higher rotational states of the molecule and the roton and maxon excitations of liquid helium phase. This likely applies here as well.

Let us finish the discussion with the unstructured component which is assigned to  $(\text{CH}_3\text{CCH})_{\geq 3}$  multimers. It is observed underneath bands 3 (isomer  $m_1$ ), 4 and 5 (isomer  $m_2$ ) of the dimer. The three latter bands are associated with the stretch of CH-groups which are not directly involved in the H-bond. The fact that features due to  $(\text{CH}_3\text{CCH})_{\geq 3}$  multimers fall in the same spectral region suggests that these multimers, as the dimer, carry “pending” CH-groups, *i.e.* CH-groups which are not involved in a H-bond. Nevertheless, the observation is surprising because these “pending” CH-groups fall in the same spectral range, regardless a dimer or a larger multimer is considered. This situation contrasts with that met with the “pending” N–H mode in the imidazole dimer and trimer studied by Lee *et al.*<sup>17</sup> These authors found that the effect of increasing the number of members in imidazole multimers is efficiently transmitted to the “pending” N–H mode through the chain of N–H...N bonds. The frequency of this mode is shifted indeed by  $-2.1 \text{ cm}^{-1}$  from the imidazole monomer to the dimer and by  $-1.5 \text{ cm}^{-1}$  from the dimer to the trimer. Here, the shift of “pending” C–H modes is comparable, although larger, when switching from the propyne monomer to the propyne dimers:  $-4.1 \text{ cm}^{-1}$  with the isomer  $m_1$  which has two equivalent “pending” C–H groups;  $-2.3$  and  $-2.9 \text{ cm}^{-1}$  for the inequivalent “pending” C–H group of isomer  $m_2$ . In contrast with imidazole, no further shift is observed with larger multimers. No attempt has been done in the present work to explore their structure by *ab initio* calculations.

## 6 Conclusion

The absorption spectrum of the propyne monomer ( $\text{CH}_3\text{CCH}$ ), dimer and  $(\text{CH}_3\text{CCH})_{\geq 3}$  multimers was explored near the CH stretch region  $\nu_1$  of the monomer, using the HELIUM

nanodroplet isolation (HENDI) technique. The central part of the work concerned a careful comparison between the experimental results and numerical simulations based on an *ab initio* investigation of the propyne dimer. The calculations were performed at the MP2 level, using several basis sets and accounting for the Basis Set Superposition Error (BSSE).

Three isomers were found for the dimer, one being *ca.* a factor two less bound than the two others. Roughly, a single H-bond is involved in the first one and two in the others. This reflects a complex landscape of the potential energy surface when several types of H-donors can form  $\text{CH} \cdots \pi$  H-bonds. In  $(\text{CH}_3\text{CCH})_2$  indeed, both the CH and  $\text{CH}_3$  groups of one  $\text{CH}_3\text{CCH}$  moiety can act as H-donor and form a H-bond with the  $\text{C}\equiv\text{C}$  group of the other. The steric effect of  $\text{CH}_3$ , larger than that of CH, creates apparently a suspended well in the potential energy surface, which stabilizes the lesser bound isomer where  $\text{CH}_3$  is the unique H-donor. To conclude, one might say that the calculations comfort the chemical intuition on the H-bond localisations.

## Conflicts of interest

There are no conflicts to declare.

## Acknowledgements

This work received partial funding from Agence nationale de la Recherche (ANR-14-CE06-0019 – ESBODYR) and Triangle de la Physique (2010-004T – NOSTADYNE-2). E. Mengesha and A. Gutiérrez-Quintanilla acknowledge partial support from Eurotalent (2015 project #259) and Triangle de la Physique (2013-0436T – REACMAQ), respectively.

## References

- 1 A. D. McNaught and A. Wilkinson, *IUPAC. Compendium of chemical terminology (the "Gold Book")*, Blackwell Scientific Publications, Oxford, 2nd edn, 1997, <https://doi.org/10.1351/goldbook>.
- 2 G. R. Desiraju and T. Steiner, *The Weak Hydrogen Bond: In Structural Chemistry and Biology*, Oxford University Press, 2001.
- 3 G. Gilli and P. Gilli, *The Nature of the Hydrogen Bond Outline of a Comprehensive Hydrogen Bond Theory*, Oxford University Press, New York, 2009, vol. 23.
- 4 M. Nishio, *Phys. Chem. Chem. Phys.*, 2011, **13**, 13873–13900.
- 5 C. Leforestier, A. Tekin, G. Jansen and M. Herman, *J. Chem. Phys.*, 2011, **135**, 234306.
- 6 M. Briant, E. Mengesha, M. A. Gaveau, B. Soep, J. M. Mestdagh and L. Poisson, *Phys. Chem. Chem. Phys.*, 2018, **20**, 2597–2605.
- 7 D. G. Prichard, R. N. Nandi and J. S. Muentner, *J. Chem. Phys.*, 1988, **89**, 115–123.
- 8 F. Stienkemeier, W. E. Ernst, J. Higgins and G. Scoles, *J. Chem. Phys.*, 1995, **102**, 615–617.
- 9 C. Callegari, K. K. Lehmann, R. Schmied and G. Scoles, *J. Chem. Phys.*, 2001, **115**, 10090–10110.
- 10 J. P. Toennies, A. F. Vilesov and K. B. Whaley, *Phys. Today*, 2001, **54**, 31–37.
- 11 M. Y. Choi, G. E. Douberly, T. M. Falconer, W. K. Lewis, C. M. Lindsay, J. M. Merritt, P. L. Stiles and R. E. Miller, *Int. Rev. Phys. Chem.*, 2006, **25**, 15–75.
- 12 J. P. Toennies, *Mol. Phys.*, 2013, **111**, 1879–1891.
- 13 M. Kaufmann, D. Leicht, R. Schwan, D. Mani, G. Schwaab and M. Havenith, *Phys. Chem. Chem. Phys.*, 2016, **18**, 28082–28090.
- 14 D. Leicht, M. Kaufmann, N. Pal, G. Schwaab and M. Havenith, *J. Chem. Phys.*, 2017, **146**, 114306.
- 15 D. Leicht, M. Kaufmann, R. Schwan, J. Schafer, G. Schwaab and M. Havenith, *J. Chem. Phys.*, 2016, **145**, 204305.
- 16 M. Y. Choi and R. E. Miller, *J. Phys. Chem. A*, 2006, **110**, 9344–9351.
- 17 S. Lee, S. J. Lee, A. Ahn, Y. Kim, A. Min, M. Y. Choi and R. E. Miller, *Bull. Korean Chem. Soc.*, 2011, **32**, 885–888.
- 18 T. Poerschke, D. Habig, G. Schwaab and M. Havenith, *Z. Phys. Chem.*, 2011, **225**, 1447–1456.
- 19 M. Briant, E. Mengesha, P. de Pujo, M.-A. Gaveau, B. Soep, J.-M. Mestdagh and L. Poisson, *Phys. Chem. Chem. Phys.*, 2016, **18**, 16414–16422.
- 20 M. Hartmann, F. Mielke, J. P. Toennies, A. F. Vilesov and G. Benedek, *Phys. Rev. Lett.*, 1996, **76**, 4560–4563.
- 21 R. Feltgen, H. Kirst, K. A. Kohler, H. Pauly and F. Torello, *J. Chem. Phys.*, 1982, **76**, 2360–2378.
- 22 K. Nauta and R. E. Miller, in *Atomic and Molecular Beams, the State of the Art*, ed. R. Campargue, Springer-Verlag, Berlin, 2001, pp. 775–792.
- 23 V. M. Horneman, G. Graner, H. Fakour and G. Tarrago, *J. Mol. Spectrosc.*, 1989, **137**, 1–8.
- 24 A. McIlroy and D. J. Nesbitt, *J. Chem. Phys.*, 1989, **91**, 104–113.
- 25 C. M. Western, *PGOPHER, a Program for Simulating Rotational Structure*, 2013.
- 26 O. Bunermann and F. Stienkemeier, *Eur. Phys. J. D*, 2011, **61**, 645–655.
- 27 H. J. Werner, P. J. Knowles, R. Lindh and F. R. Manby, *MOLPRO, version 2006.1, a package of ab initio programs*, 2012.
- 28 M. I. El Idrissi, J. Liévin, M. Herman, A. Campargue and G. Graner, *Chem. Phys.*, 2001, **265**, 273–289.
- 29 C. Møller and M. S. Plesset, *Phys. Rev.*, 1934, **46**, 618–622.
- 30 T. H. Dunning, *J. Chem. Phys.*, 1989, **90**, 1007.
- 31 R. A. Kendall, T. H. Dunning and R. J. Harrison, *J. Chem. Phys.*, 1992, **96**, 6796–6806.
- 32 S. F. Boys and F. Bernardi, *Mol. Phys.*, 1970, **19**, 553.
- 33 R. E. Zillich, Y. Kwon and K. B. Whaley, *Phys. Rev. Lett.*, 2004, **93**, 250401.